Hyperfine structure of $nP_{1/2}$ Rydberg states in ^{85}Rb

R. Cardman* and G. Raithel
Department of Physics, University of Michigan, Ann Arbor, Michigan 48109, USA

(Received 8 August 2022; accepted 2 November 2022; published 29 November 2022)

We measure the hyperfine structure of $nP_{1/2}$ Rydberg states for $n = 42$, 43, 44, and 46 using mm-wave spectroscopy on an ensemble of laser-cooled ^{85}Rb atoms. Systematic uncertainties in our measurement from the Zeeman splittings induced by stray magnetic fields and dipole-dipole interactions between two Rydberg atoms are factored in with the obtained statistical uncertainty. Our final measurement of the $nP_{1/2}$ hyperfine coupling constant is $A_{\rm HFS} = 1.443(31)$ GHz. This measurement is useful for studies of long-range Rydberg molecules, Rydberg electrometry, and quantum simulation with dipole-dipole interactions involving $nP_{1/2}$ atoms.

DOI: 10.1103/PhysRevA.106.052810

I. INTRODUCTION

The Rydberg nP_j states of Rb afford the capability of studying long-range molecular interactions in macrodimers [1–3], Rydberg-ground pairs [4,5], and, recently predicted and observed, Rydberg-ion mixtures [6–8]. Furthermore, their couplings with states of different parities are useful in understanding dipole-dipole interactions [9,10] and employing quantum electrometry of resonant rf waves via Autler-Townes splitting, observable through electromagnetically induced transparency spectroscopy [11,12]. Hyperfine interactions of the nuclear magnetic moment and electric quadrupole moment with the angular momentum of the valence electron typically are not observable in nP_j Rydberg states through laser-based spectroscopic methods due to limitations in frequency resolution (energy splittings are on the order of kHz), although hyperfine effects have been experimentally presented in Cs [13]. Millimeter-wave spectroscopy of Rydberg molecular states involving nP_j atoms could provide insights into the role of hyperfine coupling on the adiabatic potentials of the molecules, for the spectroscopic measurement is, in principle, only limited by the Rydberg-state lifetime and the rf-field interaction time. As a consequence, knowledge of the hyperfine structure (HFS) is essential for predicting these quantum behaviors.

Ongoing applications involving Rydberg nP_j states in quantum simulators, for instance in [14–16], may elicit added interest in the HFS of these states. Harnessing the HFS of Rydberg nP_j states in many-body experiments that simulate quantum phase transitions [14,17] will add a nuclear-spin degree of freedom and expand the Hilbert space to include $\{|nP_j; F', m_{F'}\rangle\}$. Rydberg states with $j = 1/2$ are preferred over $j = 3/2$ states because the former have a larger and therefore more accessible and relevant HFS than the latter. Also, the HFS of $j = 1/2$ states is insensitive to hyperfine decoupling by weak dc electric fields, and their Stark effect does not depend on $m_{F'}$. Thus, Rydberg hyperfine qubits involving $nP_{1/2}$ are expected to be more robust than ones that involve $nP_{3/2}$. Gate operations, similar to the ones performed in [18], induced by rf magnetic-field manipulations in the $\{|F', m_{F'}\rangle\}$ space would also become permissible with accurate knowledge of $A_{\rm HFS}$, obtained in the present paper.

While precision measurements of hyperfine-coupling constants have been provided before for several nP_j levels of ^{133}Cs and ^{87}Rb with principal quantum numbers $n \leqslant 13$ [19–22], for ^{85}Rb the hyperfine structure has only been measured for $nP_{3/2}$ levels with $n \leqslant 8$ [23], where the hyperfine interaction does not scale with n. In [24], the $nP_{1/2}$ HFS is observable for both ^{85}Rb and ^{87}Rb (see their Fig. 2). However, the thermal atomic beam used contributed to a significant amount of Doppler broadening, and a measurement was not provided.

In the present paper, we perform mm-wave resonance spectroscopy in the Ka and U bands on ultracold ^{85}Rb Rydberg atoms with high n. Thus, in the absence of any Doppler and transit-time broadening, we obtain Fourier-limited spectral lines of the $|nS_{1/2}, F = 3, m_F\rangle \rightarrow |nP_{1/2}, F', m_{F'}\rangle$ transitions and use the splitting between the $F' = 2$ and 3 hyperfine peaks in order to arrive at an n-independent, HFS coupling-constant $A_{\rm HFS}$ measurement for $nP_{1/2}$ Rydberg states. The spectroscopic series involves $n = 42$–44 and 46. Careful cancellation of stray magnetic fields to <5 mG is necessary to observe symmetric, Fourier-limited spectral features for both peaks. Our uncertainty budget, as a result, takes into account the role of the background magnetic field on our measurement. Additionally, we provide a systematic uncertainty arising from electric dipole-dipole interactions between $nS_{1/2}$ and $nP_{1/2}$ atoms.

II. THEORY

An alkali metal like ^{85}Rb features a single valence electron of total angular momentum **J**, spin **S**, and orbital angular momentum **L**. The nucleus of the given isotope features an intrinsic angular momentum **I** associated with the net magnetic moments of all contained nucleons. For ^{85}Rb, the nuclear spin quantum number is $I = 5/2$. In general, the hyperfine shift of

*rcardman@umich.edu

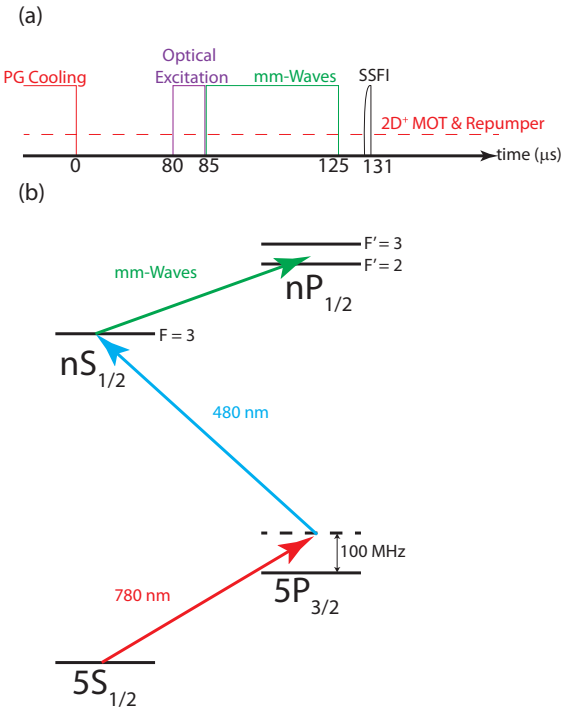

FIG. 1. (a) Timing sequence of an experimental cycle. "Optical excitation" refers to the simultaneous 780- and 480-nm pulses. The $2D^+$ MOT and repumping laser beams are always on. (b) Level diagram of ^{85}Rb states relevant to the experiment (not drawn to scale). Atoms are excited off-resonantly from the upper hyperfine level of the $5S_{1/2}$ state into the $nS_{1/2}$ Rydberg state during the optical excitation pulse. There is a statistical mixture of $F = 2$ and 3 Rydberg states after the optical excitation, but the number of atoms in the $F = 2$ states is too small to achieve an appropriate signal-to-noise ratio during the spectroscopic mm-wave pulse. Thus, the mm-wave frequency scan range is set to only probe the atoms in the $F = 3$ state.

a nP_j level with hyperfine quantum number F' is, in atomic units,

$$\Delta_{\rm HFS} = \frac{A_{\rm HFS}}{[n-\delta_{lj}(n)]^3}\langle \mathbf{I}\cdot\mathbf{J}\rangle + \frac{B_{\rm HFS}}{[n-\delta_{lj}(n)]^3}\left\langle \frac{3(\mathbf{I}\cdot\mathbf{J})^2+\frac{3}{2}\mathbf{I}\cdot\mathbf{J}-IJ(I+1)(J+1)}{2IJ(2I-1)(2J-1)}\right\rangle, \quad (1)$$

where $\delta_{lj}(n)$ is the nlj-dependent quantum defect [24], the first term describes the magnetic dipole-dipole interaction between the nucleus and Rydberg electron, and the second term quantifies the nuclear electric-quadrupole interaction. A third term, immeasurable in this type of experiment, involves magnetic-octupole interactions between the two particles [25]. For $nP_{1/2}$ states, only $A_{\rm HFS}$ is nonzero.

Due to the large extent of the Rydberg electron wave function, short-range interactions scale as $[n-\delta_{lj}(n)]^{-3}$ [26]. Thus, the measured splitting $\nu_{\rm HFS}$ between $F' = 2$ and 3 can be expressed as

$$\nu_{\rm HFS} = \frac{3A_{\rm HFS}}{[n-\delta_{lj}(n)]^3}, \quad (2)$$

where the units of $A_{\rm HFS}$ are GHz.

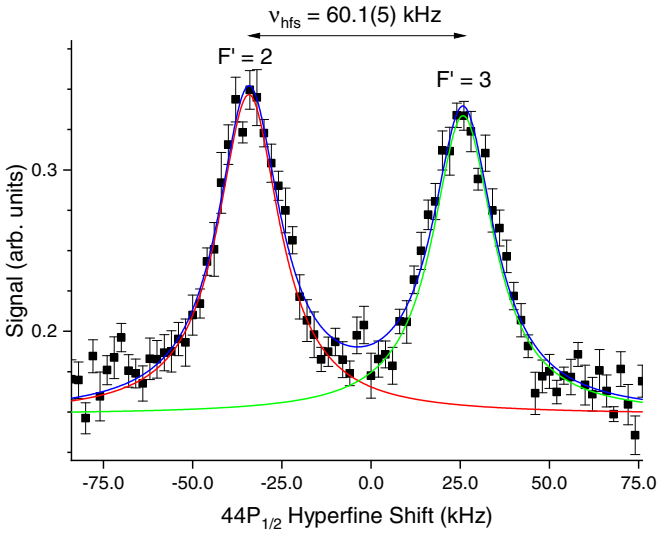

FIG. 2. Single-photon resonance spectrum of the $|44S_{1/2}, F = 3\rangle \rightarrow |44P_{1/2}, F'\rangle$ transition using mm waves. The spectrum shown is an arithmetic mean of eight individual spectra. Each individual spectrum is averaged over 400 experimental cycles. On the frequency axis, we show the $44P_{1/2}$ hyperfine shifts for each F' level with respect to the center-of-gravity transition frequency, $\nu_0 = 45.113\,624$ GHz, i.e., the frequency of the $|44S_{1/2}, F = 3, m_F\rangle \rightarrow |44P_{1/2}\rangle$ transition with the $44P_{1/2}$ hyperfine structure removed. Each scatter point corresponds to a frequency step size of 2 kHz. Signal error bars for the scatter points indicate the standard error of the mean over the eight individual points acquired. In this spectrum, the total detected count rate is below two ions per experimental cycle. The solid curves are the double- and individual-Lorentzian fit functions from which the peak centers are acquired to measure the HFS splittings. Measured linewidths are 21(1) kHz for both peaks.

III. METHODS

In our experiment, a slow atomic beam of ^{85}Rb prepared by a continuously operating two-dimensional or higher ($2D^+$) magneto-optical trap (MOT) [27] is captured and cooled via polarization gradients in the σ^+-σ^- configuration [28] for 14.2 ms. We leave the $2D^+$ MOT laser beams and all repumping beams on throughout the duration of the experiment. The D_2-molasses cooling light is switched off for 80 μs before 5-μs-long optical excitation beams are switched on. These beams produce $nS_{1/2}$ Rydberg atoms used for the mm-wave spectroscopy, where $n = 42$–44 and 46. A 40-μs mm-wave pulse drives the $|nS_{1/2}, F = 3, m_F\rangle \rightarrow |nP_{1/2}, F' = 2 \text{ or } 3, m_{F'}\rangle$ transitions necessary for determining the hyperfine splitting. At the end of the mm-wave exposure time, an electric field is smoothly ramped up to 100–150 V/cm in 1 μs for state-selective field ionization of the $nS_{1/2}$ and $nP_{1/2}$ levels [26]. $^{85}Rb^+$ counts are detected with a microchannel-plate detector. A timing sequence for the experimental cycle is given in Fig. 1(a).

Optical excitation from the upper hyperfine level of the ground state is provided in the form of an off-resonant, two-photon transition using 780- and 480-nm pulses, described in the quantum-state diagram of Fig. 1(b). A 780-nm external-cavity diode laser (ECDL) is tuned 100 MHz above

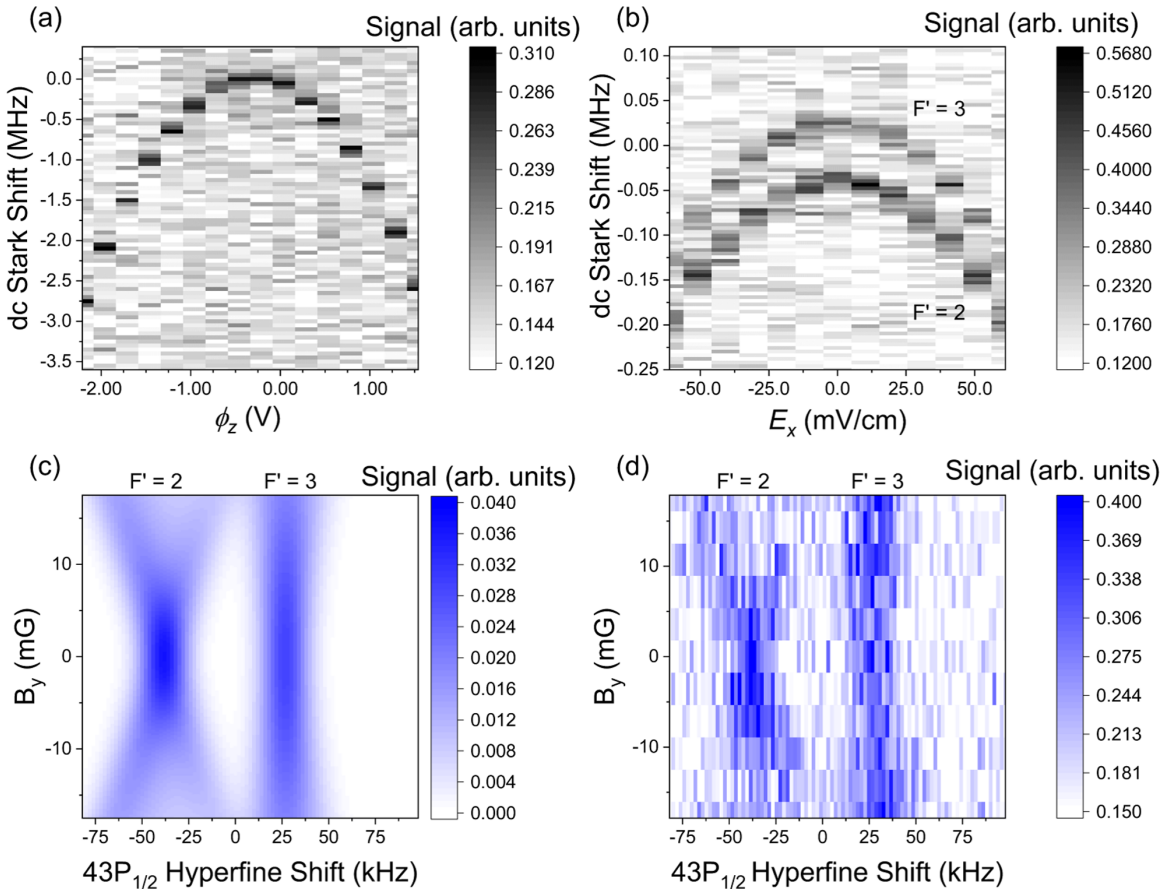

FIG. 3. This figure explains the static electromagnetic-field zeroing process necessary for a HFS measurement. (a) Map of dc Stark shifts on the $|44S_{1/2}\rangle \rightarrow |44P_{1/2}\rangle$ transition as a function of applied potential ϕ_z on plate electrodes in order to find the voltage that cancels shifts from stray electric fields along the z direction. The differential dc polarizability between the two states is $\alpha_{44P_{1/2}} - \alpha_{44S_{1/2}} = 9.564$ kHz/(V/m)^2. Here, the mm-wave frequency steps are not resolved enough to observe the HFS splitting. (b) Verification that the hyperfine splitting is not affected by electric fields smaller than 60 mV/cm. The $|43S_{1/2}, F = 3\rangle \rightarrow |43P_{1/2}, F'\rangle$ spectra are plotted as a function of applied electric field E_x in the x direction with stray fields canceled in the other two directions. (c) Calculated Zeeman splitting of the $|43S_{1/2}, F = 3\rangle \rightarrow |43P_{1/2}, F'\rangle$ transitions for $F' = 2$ and 3. This calculation is for the case that the applied magnetic field is perpendicular (y direction) to the mm-wave polarization. (d) Experimental analog to our calculation.

the uppermost hyperfine level of the $5P_{3/2}$ state, while a 960-nm ECDL, amplified and doubled to make 480-nm light, is tuned to make up the resonance with the Rydberg state. Polarizations of the optical excitation beams and atomic sample, as well as the blue-detuning of the 780-nm laser from the uppermost hyperfine level of the $5P_{3/2}$ state, result in significantly more Rydberg-atom population in $|nS_{1/2}, F = 3, m_F\rangle$ than $|nS_{1/2}, F = 2, m_F\rangle$. Therefore, we perform our mm-wave spectroscopy only on the $F = 3$ hyperfine levels for all n studied.

TABLE I. Summary of HFS splittings and derived $A_{\rm HFS}$ using Eq. (2) and $\delta_0 = 2.654\,884\,9(10)$, $\delta_2 = 0.2900(6)$ [24].

n	$\nu_{\rm HFS}$ (kHz)	$A_{\rm HFS}$ (GHz)
42	72.7(6)	1.476(12)
43	65.3(6)	1.429(13)
44	60.1(5)	1.416(12)
46	54(1)	1.466(27)
$A_{\rm HFS}$, weighted average (GHz)		1.443
Statistical uncertainty (GHz)		0.007

The mm waves are synthesized by an Agilent MXG Analog Signal Generator (Model N5183A) that is referenced to an SRS Model FS725 rubidium frequency standard. For spectroscopy of $n = 42$–44, the synthesized mm waves are frequency doubled by a SAGE Model SFA-192KF-S1 active X2 multiplier and broadcast from $\simeq 40$ cm to the $nS_{1/2}$ Rydberg atoms with a horn antenna. We do not double the mm waves at 39.121 GHz for the $|46S_{1/2}, F = 3, m_F\rangle \rightarrow |46P_{1/2}, F', m_{F'}\rangle$ spectrum and directly connect the synthesizer to a standard-gain horn antenna, located $\simeq 30$ cm from the spectroscopic interaction region, with a 20-dBi directivity.

IV. RESULTS

Spectra of the $|nS_{1/2}, F = 3, m_F\rangle \rightarrow |nP_{1/2}, F', m_{F'}\rangle$ transition were acquired for each n in the $n = 42$–44 and 46 series. A double Lorentzian was fit to an arithmetic average of eight experimental scans of the mm-wave frequency over the two

hyperfine lines. In order to determine ν_{HFS} from our data, we take the difference between the line centers of the Lorentzian fit functions. The uncertainties in the line centers were added in quadrature and used as the uncertainty in the HFS splitting, $\delta\nu_{\mathrm{HFS}}$. Figure 2 shows a typical spectrum obtained in this paper. The linewidths are at the level of the Fourier limit ($0.89/40\,\mu\mathrm{s} = 22\,\mathrm{kHz}$), meaning the Rabi frequencies of the transitions are in the range of 10 kHz, preventing any observable ac Stark shifts.

Once we obtain ν_{HFS}, we use the δ_0 and δ_2 quantum-defect values for Rb $nP_{1/2}$ measured in [24] and the Rydberg-Ritz equation [26] to derive a measurement for A_{HFS} using Eq. (2). These quantities are $\delta_0 = 2.654\,884\,9(10)$ and $\delta_2 = 0.2900(6)$. Because the uncertainties in δ_0 and δ_2 lead to shifts much smaller than our measurement uncertainties, we neglect them in our uncertainty budget. Thus, $\delta A_{\mathrm{HFS}}/A_{\mathrm{HFS}} = \delta\nu_{\mathrm{HFS}}/\nu_{\mathrm{HFS}}$. Table I lists ν_{HFS} and A_{HFS} for a given n in the range $n = 42$–44 and 46. A weighted average and uncertainty over all n provide a final value for A_{HFS} and a statistical uncertainty, also included in the table.

V. DISCUSSION

Symmetry of our observed spectral lines indicates that background electric- and magnetic-field inhomogeneities are negligible. A set of six orthogonal plate electrodes situated in our science chamber is used to cancel electric fields below 50 mV/cm by observing shifts in $|nS_{1/2}\rangle \rightarrow |nP_{1/2}\rangle$ spectra as a function of applied electric field; a map of these spectra is shown along the z axis in Fig. 3(a) for $n = 44$. Figure 3(b) displays a more resolved map for $n = 43$ with an applied field along the x direction. Electric fields contribute no systematic shift in the HFS splitting because the $nP_{1/2}$ Rydberg states lack a tensor polarizability that would otherwise cause distortions in the $F' = 2$ and 3 peaks as a result of $|m_{F'}|$ splittings. Therefore, both F' states and all $|m_{F'}|$ undergo the same dc Stark shifts leaving ν_{HFS} insensitive to stray electric fields. This insensitivity is verified in Fig. 3(b) for $n = 43$, where we apply electric-field E_x magnitudes up to 60 mV/cm and scan over both hyperfine peaks of the $43P_{1/2}$ state. Inhomogeneous broadening from position-dependent electric fields within the atom cloud is the only possible dc Stark effect, which is negligible as exhibited by the line symmetries and linewidths near the Fourier limit of 22 kHz. Excessive magnetic fields within the interaction region on the other hand do distort measurements of ν_{HFS} from the Zeeman splittings of the m_F and $m_{F'}$ sublevels, as seen in the following paragraph.

Three pairs of externally located Helmholtz coils apply homogeneous magnetic fields to eliminate Zeeman broadening and splitting of the F' states [29]. Expected and observed behaviors of the Zeeman splittings for $n = 43$ are shown in Figs. 3(c) and 3(d), respectively, for the case of a magnetic field perpendicular to the mm-wave polarization. Our stray magnetic fields are reduced down to a magnitude no greater than 5 mG. In order to quantify the possible systematic uncertainties from any leakage within this range, we take the standard error of the mean (SEM) in a sample of splittings at $n = 43$ by offsetting our compensation magnetic fields within 10 mG of the cancellation values in all three directions x, y, and z independently. A similar analysis was done in the context of measuring the $nS_{1/2}$ HFS for ^{85}Rb Rydberg states [29]. This distribution is presented in Fig. 4. Our SEM yields $\delta\nu_{\mathrm{HFS}} = 0.6$ kHz at $n = 43$ and $\delta A_{\mathrm{HFS}} = 13$ MHz.

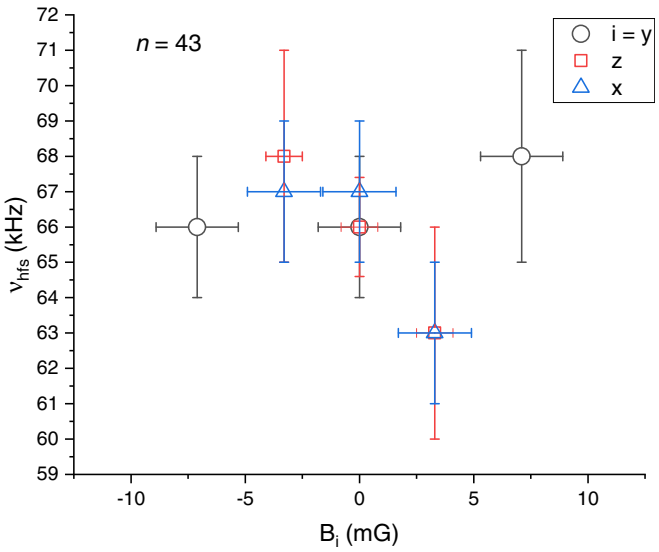

FIG. 4. Measured ν_{HFS} of $43P_{1/2}$ for given applied magnetic fields in all three spatial dimensions. The SEM of all nine ν_{HFS} is used as the systematic $\delta\nu_{\mathrm{HFS}}$ from potential stray magnetic fields. Magnetic-field uncertainties arise from noise in our current sources.

We also take into account shifts from dipole-dipole interactions between one atom with an internal state of $nS_{1/2}$ and another with that of $nP_{1/2}$. The interaction energy of such a Rydberg-atom pair is C_3/R^3, with a dispersion coefficient C_3 and an internuclear separation R. In Fig. 5, we exhibit that

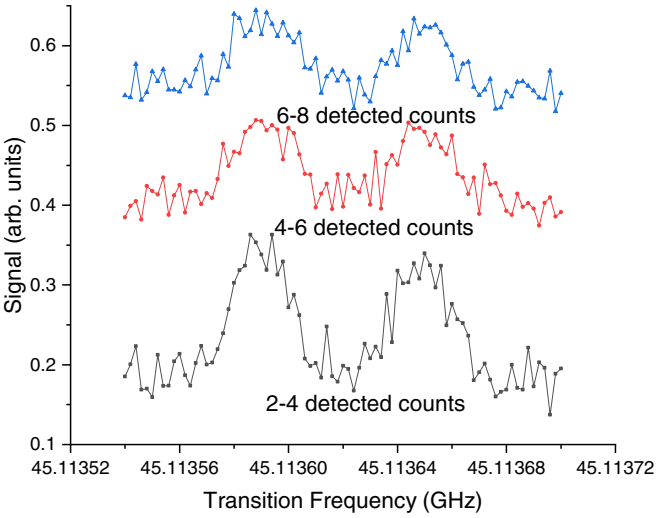

FIG. 5. In this series, the $44P_{1/2}$ HFS is measured for three different bins of total detected ion counts from field-ionized Rydberg atoms. The increase in count rate is achieved by starting the optical excitation 5–10 μs earlier to prolong the laser pulse duration. Because the atomic density is rising proportionally with the count rate, the dipole-dipole shifts, if they are significant, should increase as well. There is no apparent dipole-dipole shift over 1 kHz, implying that the atomic spacing must be at a minimum of 120 μm.

TABLE II. Uncertainty budget for a measurement of A_{HFS}.

Source	δA_{HFS} (GHz)
Dipole-dipole interactions	0.027
Stray magnetic fields	0.013
Statistical uncertainty	0.007

the shift in ν_{HFS} does not exceed 1 kHz for $n = 44P_{1/2}$, as the maximum ion-count rate, and therefore density, is increased by a factor 4 by prolonging the optical excitation time up to 15 μs. All measurements in Table I were taken with fewer than three detected total counts. An upper limit of the C_3 coefficient is estimated to be 1.7 GHz $\mu\mathrm{m}^3$ for $n = 44$ by finding and fitting adiabatic potentials of Rydberg-Rydberg molecules [30]. This estimate implies that the atomic spacing is $R \gtrsim 120\,\mu$m and the systematic uncertainty in A_{HFS} from dipole-dipole interactions has an upper limit of 27 MHz. Higher-order Rydberg-Rydberg interactions, such as van der Waals shifts between two atoms of the same internal state, are at the order of 1 mHz or less for these n and therefore are not included in our overall uncertainty budget [29].

We present our uncertainty budget in Table II. Adding the three sources in quadrature, we find the overall uncertainty to be $\delta A_{\mathrm{HFS}} = 31$ MHz.

In summary, we measured the hyperfine coupling constant A_{HFS} for Rydberg-$nP_{1/2}$ states of ^{85}Rb using mm-wave spectroscopy with Fourier-limited linewidths. Our precision in A_{HFS} is mainly limited by the estimated lower limit of atomic spacing within our Rydberg cloud that may lead to dipole-dipole interactions. In addition to our measurement's applicability for investigating ultracold Rydberg chemistry [1–8] and dynamic electric-field sensing of rf waves with thermal Rydberg atoms [11–13], the HFS of $nP_{1/2}$ states can possibly be included in several experiments and models for quantum simulation [14–17].

ACKNOWLEDGMENTS

This work was supported by NSF Grants No. PHY-2110049 and No. PHY-1806809 and NASA Grant No. NNH13ZTT002N. R.C. acknowledges support from the Rackham Predoctoral Fellowship.

[1] C. Boisseau, I. Simbotin, and R. Côté, Phys. Rev. Lett. **88**, 133004 (2002).
[2] S. Hollerith, J. Zeiher, J. Rui, A. Rubio-Abadal, V. Walther, T. Pohl, D. M. Stamper-Kurn, I. Bloch, and C. Gross, Science **364**, 664 (2019).
[3] S. Hollerith, J. Rui, A. Rubio-Abadal, K. Srakaew, D. Wei, J. Zeiher, C. Gross, and I. Bloch, Phys. Rev. Res. **3**, 013252 (2021).
[4] T. Niederprüm, O. Thomas, T. Eichert, C. Lippe, J. Pérez-Ríos, C. H. Greene, and H. Ott, Nat. Commun. **7**, 12820 (2016).
[5] T. Niederprüm, O. Thomas, T. Eichert, and H. Ott, Phys. Rev. Lett. **117**, 123002 (2016).
[6] A. Duspayev, X. Han, M. A. Viray, L. Ma, J. Zhao, and G. Raithel, Phys. Rev. Res. **3**, 023114 (2021).
[7] M. Deiß, S. Haze, and J. Hecker Denschlag, Atoms **9**, 34 (2021).
[8] N. Zuber, V. S. Anasuri, M. Berngruber, Y.-Q. Zou, F. Meinert, R. Löw, and T. Pfau, Nature (London) **605**, 453 (2022).
[9] W. Li, P. J. Tanner, and T. F. Gallagher, Phys. Rev. Lett. **94**, 173001 (2005).
[10] S. Ravets, H. Labuhn, D. Barredo, L. Béguin, T. Lahaye, and A. Browaeys, Nat. Phys. **10**, 914 (2014).
[11] C. L. Holloway, J. A. Gordon, S. Jefferts, A. Schwarzkopf, D. A. Anderson, S. A. Miller, N. Thaicharoen, and G. Raithel, IEEE Trans. Antennas Propag. **62**, 6169 (2014).
[12] D. A. Anderson, R. E. Sapiro, L. F. Gonçalves, R. Cardman, and G. Raithel, Phys. Rev. Appl. **17**, 044020 (2022).
[13] F. Ripka, C. Lui, M. Schmidt, H. Kubler, and J. P. Shaffer, in *Optical and Quantum Sensing and Precision Metrology II*, edited by J. Scheuer and S. M. Shahriar, International Society for Optics and Photonics, Vol. PC12016 (SPIE, Bellingham, WA, 2022), pp. 102–107.
[14] A. Browaeys and T. Lahaye, Nat. Phys. **16**, 132 (2020).
[15] S. Kanungo, J. Whalen, Y. Lu, M. Yuan, S. Dasgupta, F. Dunning, K. Hazzard, and T. Killian, Nat. Commun. **13**, 972 (2022).
[16] M. Khazali, Quantum **6**, 664 (2022).
[17] P. Scholl, M. Schuler, H. J. Williams, A. A. Eberharter, D. Barredo, K.-N. Schymik, V. Lienhard, L.-P. Henry, T. C. Lang, T. Lahaye *et al.*, Nature (London) **595**, 233 (2021).
[18] S. Ma, A. P. Burgers, G. Liu, J. Wilson, B. Zhang, and J. D. Thompson, Phys. Rev. X **12**, 021028 (2022).
[19] G. Belin and S. Svanberg, Phys. Lett. A **47**, 5 (1974).
[20] G. Belin, L. Holmgren, and S. Svanberg, Phys. Scr. **13**, 351 (1976).
[21] G. Belin, L. Holmgren, and S. Svanberg, Phys. Scr. **14**, 39 (1976).
[22] J. Farley, P. Tsekeris, and R. Gupta, Phys. Rev. A **15**, 1530 (1977).
[23] G. zu Putlitz and K. V. Venkataramu, Zeitschrift für Physik A: Hadrons and Nuclei **209**, 470 (1968).
[24] W. Li, I. Mourachko, M. W. Noel, and T. F. Gallagher, Phys. Rev. A **67**, 052502 (2003).
[25] D. A. Steck, Rubidium 85 D line data, https://steck.us/alkalidata/rubidium85numbers.pdf (2008).
[26] T. F. Gallagher, *Rydberg Atoms* (Cambridge University, New York, 2005), Vol. 3.
[27] K. Dieckmann, R. J. C. Spreeuw, M. Weidemüller, and J. T. M. Walraven, Phys. Rev. A **58**, 3891 (1998).
[28] J. Dalibard and C. Cohen-Tannoudji, J. Opt. Soc. Am. B **6**, 2023 (1989).
[29] A. Ramos, R. Cardman, and G. Raithel, Phys. Rev. A **100**, 062515 (2019).
[30] X. Han, S. Bai, Y. Jiao, L. Hao, Y. Xue, J. Zhao, S. Jia, and G. Raithel, Phys. Rev. A **97**, 031403(R) (2018).